We are IntechOpen,
the world's leading publisher of
Open Access books
Built by scientists, for scientists

6,900
Open access books available

185,000
International authors and editors

200M
Downloads

154
Countries delivered to

Our authors are among the

TOP 1%
most cited scientists

12.2%
Contributors from top 500 universities

CLARIVATE ANALYTICS
BOOK CITATION INDEX
INDEXED

WEB OF SCIENCE™

Selection of our books indexed in the Book Citation Index
in Web of Science™ Core Collection (BKCI)

Interested in publishing with us?
Contact book.department@intechopen.com

Numbers displayed above are based on latest data collected.
For more information visit www.intechopen.com

Silicide Nanowires from Coordination Compound Precursors

John Philip
The Catholic University of America
USA

1. Introduction

In the last two decades there has been a great interest in the synthesis and characterization of one-dimensional materials. A variety of inorganic materials have been prepared in the form of nanowires and nanobelts with a diameter of a few nanometer and lengths going up to several hundreds of microns (Xia et al., 2003). The two main techniques used for nanowire growth are vapor-assisted (Wagner, 1964) and solution-based growth (Stejny, 1981; Stejny, 1979; Kruyt & Arkel, 1923; Gates et al., 2002; Mayers & Xia, 2002; Messer et al., 2000; Song et al., 2001) processes. Nanowires, nanorods and nanobelts constitute an important class of 1D nanostructures, which provide models to study the relationship between electrical transport, optical, magnetic and combined properties such as electro-optic and magneto-electronic properties with dimensionality and size confinement.

In recent decades strong interest has been drawn to explore silicides (Murarka, 1983; Miglio & d'Heurle, 2000), which are chemical compounds of silicon with different metals. Considerable amount of studies are carried out on transition metal silicides such as $CoSi_2$, NiSi, MnSi, $CrSi_2$, FeSi (Maex & Rossum, 1995). The magnetic properties of MnSi and FeSi are studied extensively. MnSi has a helical spin structure at low fields below 29 K and it is paramagnetic above that temperature (Ishikawa et al., 1976; Belitz, 1999). CrSi and NiSi are either weakly paramagnetic or diamagnetic. The transition-metal monosilicides such as MnSi, CoSi and FeSi are a group of highly correlated electron materials (Aeppli & DiTusa, 1999; Riseborough, 2000). In the case of MnSi, application of external magnetic fields results in field-induced phase transitions from the helimagnetic phase to a conical spin structure at low fields and then to a ferromagnetic state at higher magnetic fields (Ishikawa et al., 1976; Belitz, 1999). The temperature dependence of high field magnetization of field-induced ferromagnetic states of MnSi shows signatures indicating the role of both spin wave excitations and stoner band excitations related to itinerant electron ferromagnetism (Aeppli & DiTusa, 1999). In another manganese-based silicide, Mn_5Si_3, the magnetic structure has been studied for many years (Lander et al., 1967; Brown & Forsyth, 1995; Silva et al., 2002). Mn_5Si_3 shows two different antiferromagnetic configurations with a low temperature highly non-collinear phase (Lander et al., 1967; Brown & Forsyth, 1995; Silva et al., 2002). It was previously reported that antiferromagnetic Mn_5Si_3 can be driven into a ferromagnetic or ferrimagnetic state by insertion of carbon into the voids of Mn octahedra of the hexagonal structure (Sénateur, 1967). Thin films of $Mn_5Si_3C_x$ with $x = 0.8$ have a Curie temperature $T_C = 350$ K (Sürgers, 2003) well above room temperature. FeSi is a Kondo insulator (Aeppli &

DiTusa, 1999), a class of heavy-electron compounds exhibiting Kondo lattice behavior at room temperature.

Semiconducting silicides, such as the higher manganese silicides (HMS) $MnSi_{1.7}$, $CrSi_2$ have a high potential for thermoelectric applications (Vining, 1995; Borisenko, 2000). Additionally, such semiconducting silicides $FeSi_2$, $MnSi_{1.7}$ and Ru_2Si_3 are reported to have a direct band gap, which makes them attractive for optoelectronic application (Borisenko, 2000). Most of the recent investigations of semiconducting silicides have been focused on the thin films of $FeSi_2$ and $CrSi_2$. Semiconducting higher manganese silicides $MnSi_x$ with a composition x varying from 1.67 to 1.75 are the most promising candidates for understanding the fundamental physics as well as for applications such as microelectronics, spintronics and thermoelectrics. There exist a number of tetragonal HMS phases, Mn_4Si_7, $Mn_{11}Si_{19}$, $Mn_{15}Si_{26}$, etc., which differ slightly in their composition (Schwomma et al., 1964; Flieher et al., 1967).

Most of the studies on silicides are carried out either in bulk or in thin films. Recently several groups have explored the growth of silicide nanostructures using a variety of methods. In chemical vapor deposition (CVD) method the main precursor used is $M(SiCl_3)_x(CO)_y$, where M = Fe, Mn or Co (Aylett & Colquhoun, 1977; Novak et al., 1997; Schmitt et al., 2010). CVD utilizes the vapor-liquid-solid (VLS) mechanism to the growth of silicide nanowires. Wagner studied the growth of millimeter-sized Si whiskers in the presence of Au particles, involving the VLS process (Wagner, 1964). According to this mechanism, the anisotropic crystal growth is promoted by the presence of the liquid alloy/solid interface. This mechanism has been widely accepted and applied for understanding the growth of various nanowires.

2. Growth of silicide nanowires

In this chapter, we describe the synthesis, structure and properties of nanowires of silicides with manganese as one of the components. We have grown silicide nanowires using a class of coordination compound precursors called β-diketone chelates. This class of precursor can be used for growing a variety of silicides, including Mn-Si-C. This chapter will be organized as follows: First we will discuss the 1) Mn-based beta-diketone chelates (Kang et al., 2009), 2) then we will describe the synthesis of Mn_5SiC nanostructures and its structural, magnetic properties (Kang et al., 2009), 3) growth of Mn_5SiC nanostructures with different boron concentration and describe their magnetic and transport properties (Kang et al., 2010) and finally 4) the growth of higher manganese silicide, $Mn_{15}Si_{26}$ using a similar precursor. We will discuss the electrical transport properties of $Mn_{15}Si_{26}$ nanostructures and show that for the first time we have grown semiconducting $Mn_{15}Si_{26}$ nanostructures.

2.1 Coordination compound precursors

Precursors that we have used for manganese are manganese beta-diketone chelates (Walker & Li, 1965; Cotton & Holm, 1960). We have used two different Mn beta-diketone chelates (Figure 1), bis(1,1,1,5,5,5-hexafluoro-2,4-pentanedionato) manganese(II) and bis(4,4,4-trifluoro-1-phenyl-1,3-butanedionato) manganese(II) complexes. The precursor with phenyl group is used for synthesizing Mn_5SiC and the other is used for the growth of manganese silicides with varying concentrations of Mn and Si by controlling the flux of manganese and the temperature of the growth.
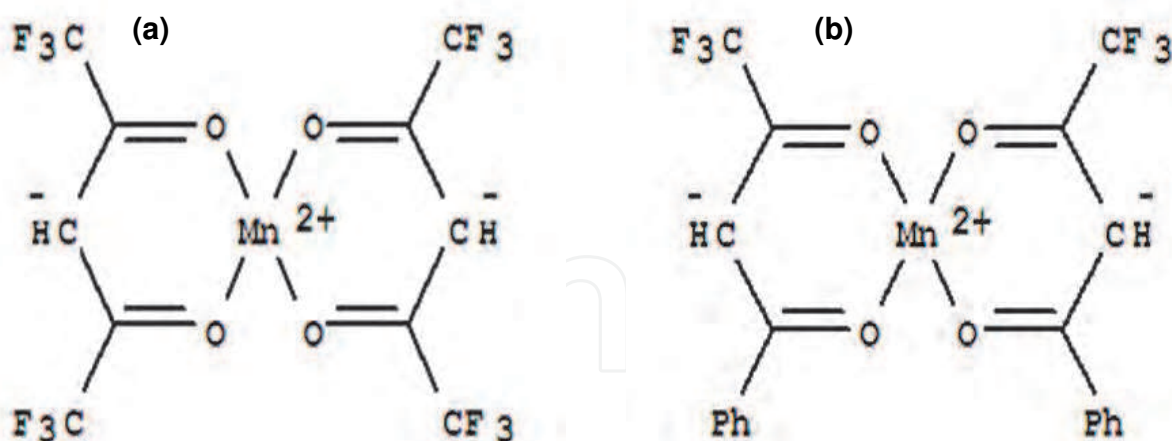
Fig. 1. (a) bis(1,1,1,5,5,5-Hexafluoro-2,4-pentanedionato) manganese(II) complex (b) bis(4,4,4-trifluoro-1-phenyl-1,3-butanedionato) manganese(II) complex.

2.2 Growth of Mn$_5$SiC nanowires

We have grown Mn$_5$SiC nanowires using a precursor (Figure 1a) for Mn and C. Si (111) substrates were used as the Si source. A coordination complex precursor bis(4,4,4-trifluoro-1-phenyl-1,3-butanedionato) manganese(II), Mn(PhC(O)CHC(O)CF$_3$)$_2$, was used as a source for both Mn and C. The synthesis of the precursor [hereafter referred to as Mn-phenyl-complex] was carried out using the general procedure outlined in Walker & Li, 1965; Cotton & Holm, 1960. The native oxide of the Si substrate was etched away using dilute HF; a thin layer of Au nanoparticles (average size of 20 nm) was sprayed onto the etched Si surface; and the substrates were placed inside a quartz tube in a horizontal tube furnace. The system was pumped down to 10 mtorr before flowing an ultra-high purity Ar and H$_2$ gas mixture (10 % H$_2$) at a rate of 1000 standard cm^3 per minute. Two heating zones with temperatures of 350 °C and 1050 °C were used for vaporization of the precursor and nanowire growth, respectively. The Si substrates were placed at the center of the furnace with the precursor at about 20 cm away. When the center of the furnace reached the set point of 1050 °C, the Mn phenyl-complex was hot (300 – 400 °C) enough to vaporize; Mn phenyl-complex is a highly volatile compound. The vapor-phase precursors were carried by the Ar-H$_2$ mixture to the center of the furnace where they reacted with silicon from the substrates. The reaction was continued under these conditions for 2 hrs before the furnace was allowed to cool to room temperature while maintaining the gas flow. Nanowires with diameters in the range of 2 - 100 nm can be grown using this method (Figure 2). Figure 3 shows the x-ray diffraction pattern of the nanowires. All of the grown nanowires exhibit orthorhombic structure with Cmc21 space group. The lattice parameters for the grown nanowires are a = 10.198, b = 8.035 and c = 7.630 Å respectively. The high-resolution transmission electron microscopy (TEM) image in Figure 4(a) shows the (331) lattice planes of orthorhombic Mn$_5$SiC structure. The selected area electron diffraction pattern can also be indexed based on the same structure. We have measured the magnetic properties of these nanowires using a Quantum design MPMS system. These nanostructures exhibit ferromagnetic behavior (Figure 5) both at 300 and 10 K.
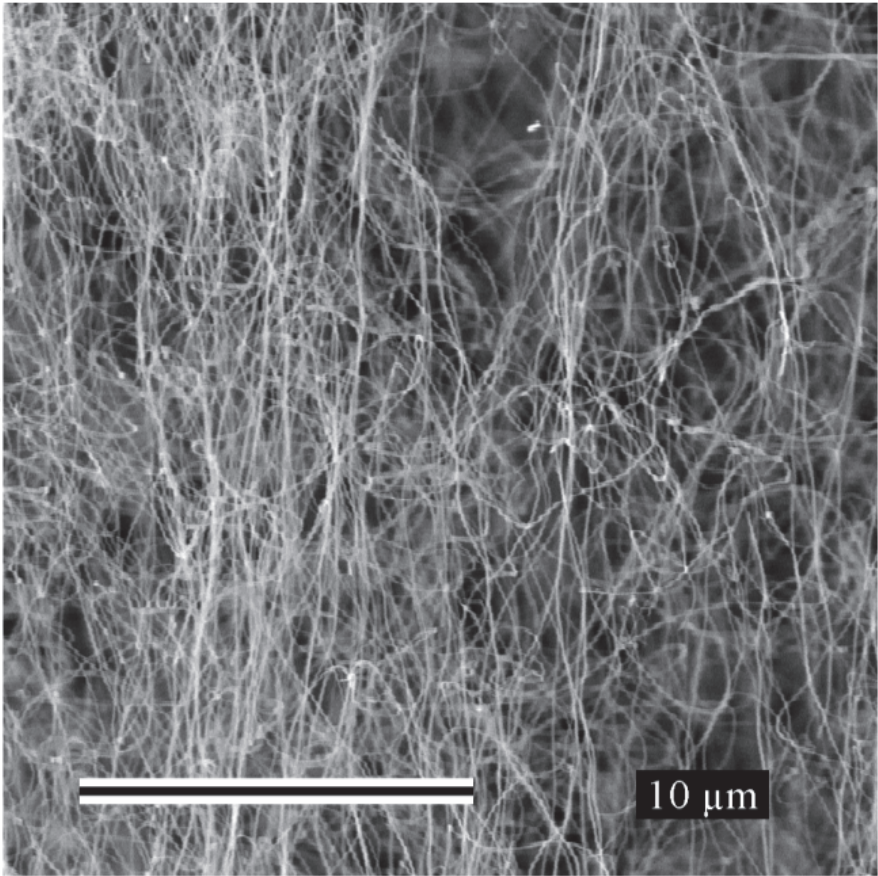
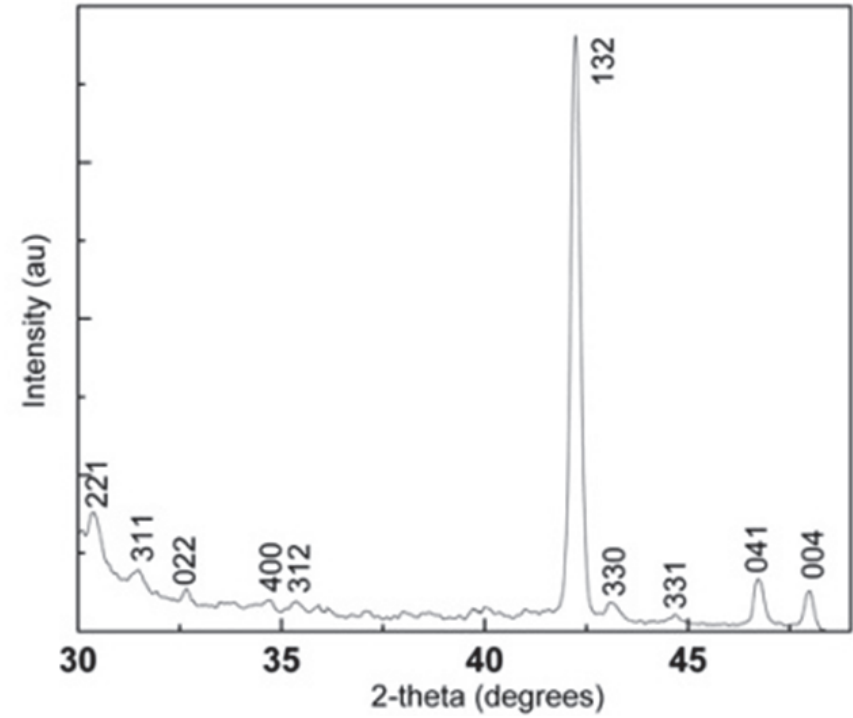Fig. 2. Scanning electron microscopy image of Mn$_5$SiC nanowires.

Fig. 3. X-ray diffraction pattern of as-grown Mn$_5$SiC nanowires. The pattern is indexed based on orthorhombic Mn$_5$SiC structure.
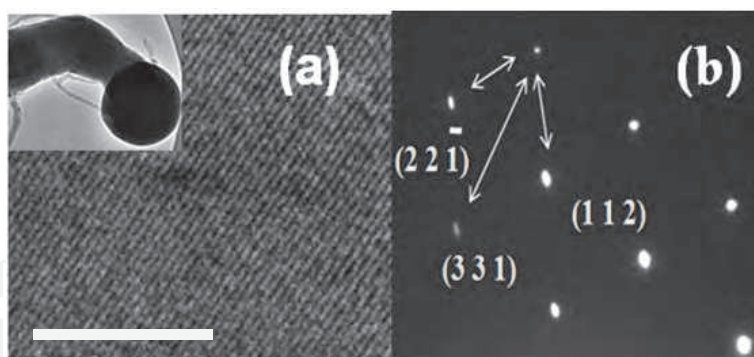
Fig. 4. (a) High resolution TEM image displays the (331) lattice planes of Mn_5SiC structure. The scale bar is 2.0 nm. Inset: TEM image showing catalyst nanoparticle at tip of the nanowire. (b) selected area electron diffraction pattern can be indexed to an orthorhombic Mn_5SiC structure.
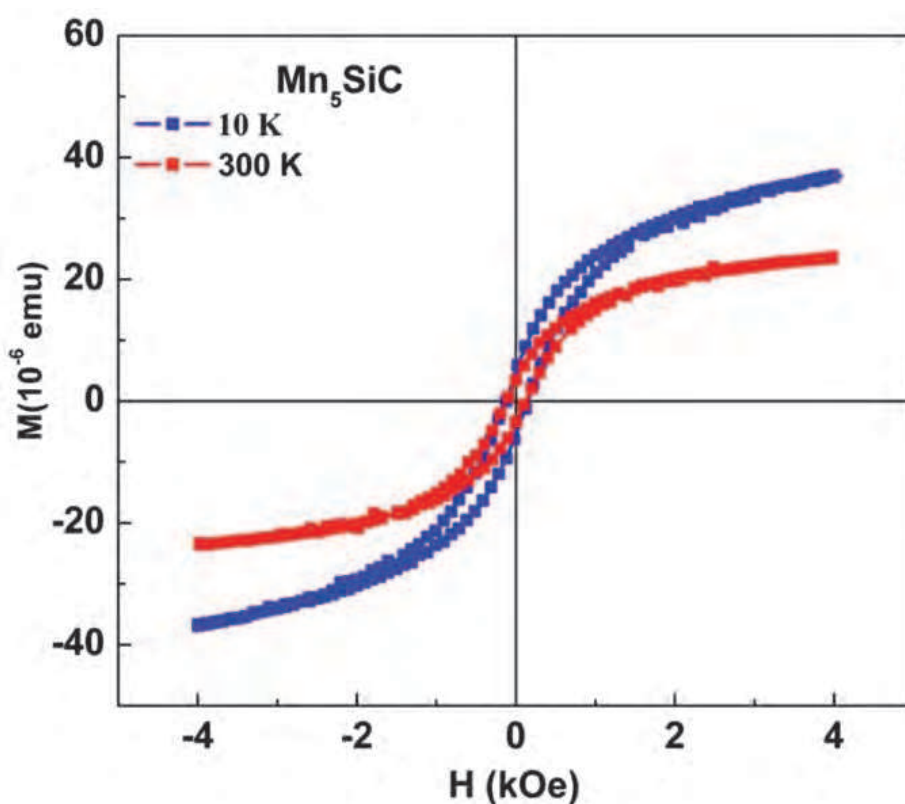

Fig. 5. Hysteresis loops of as-grown Mn_5SiC nanowire cluster at 300 and 10 K.

2.3 Boron-doped Mn₅SiC nanowires

Mn_5SiC nanowires exhibit ferromagnetic behavior and the T_c appears to be higher than 400 K. In order to clearly understand the ferromagnetic behavior and the magneto-transport properties we have grown Mn_5SiC nanostructures from differently boron-doped silicon substrates. The growth of boron-incorporated Mn_5SiC nanowires was carried out using chemical vapor deposition involving a coordination complex precursor for Mn and C. From the earlier discussion on CVD, the only difference here is in choosing the silicon substrate. We have used boron-doped silicon substrates with (100) orientation. The silicon substrate is

used as the source for silicon in boron-incorporated Mn_5SiC nanostructures. We have used silicon substrates with three different boron doping for the growth of these nanowires. The boron doping concentrations were 2×10^{17}, 5×10^{18} and 5×10^{19} /cm^3 respectively. The nanowires grown from these substrates will be referred to as low, medium and heavy-boron incorporated nanowires (LBNW, MBNW and HBNW) respectively. Highly dense boron-incorporated Mn_5SiC nanowires were grown as shown in Figure 6. Nanowire size ranges from 50 – 100 nm. Figure 7 illustrates the x-ray diffraction pattern of nanowires grown from three different silicon substrates. All of the grown nanowires exhibit orthorhombic structure with Cmc21 space group. The lattice parameters for the grown nanowires are a = 10.198, b = 8.035 and c = 7.630 Å respectively. There is no systematic shift of the peaks with boron incorporation to elucidate whether there is a lattice volume change. It would be possible that the varying size range (50 -100 nm) and the stress in the nanowires on different sets also contribute to the line width and broadening (Cullity, 1977). Gold nanoparticles (100 nm) were used as catalyst for the nanowire growth, in addition to the formation of Mn_5SiC nanowires, formation of a small fraction of Au_5Si_2 particles was also observed. The peaks corresponding to the Au_5Si_2 phase are marked in Figure 7. The selected area electron diffraction pattern obtained from a representative nanowire is indexed to an orthorhombic Mn_5SiC structure. The energy-dispersive x-ray analysis using high-resolution transmission electron microscopy reveals that the nanowires consist of Mn, Si and C and their ratio
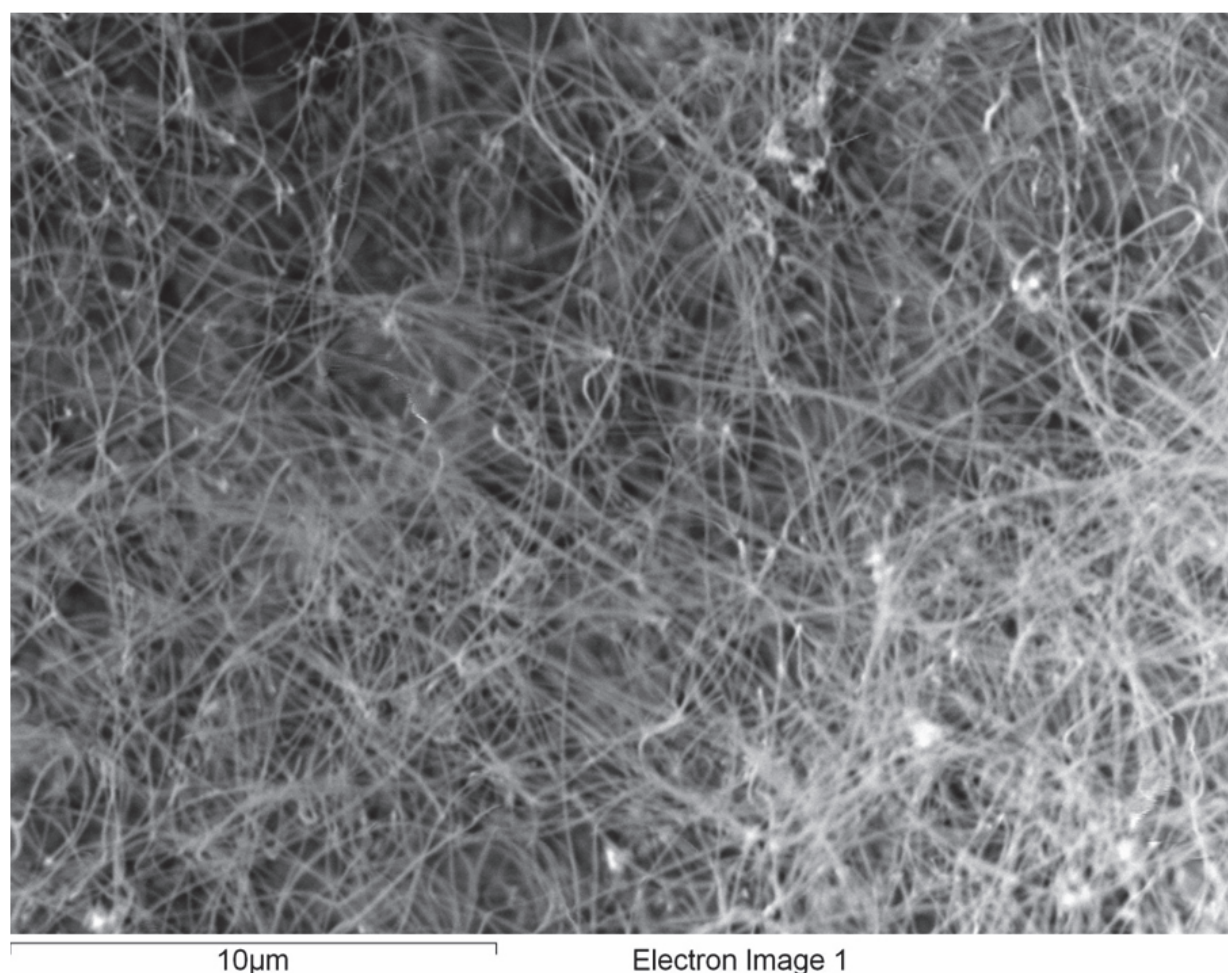

10μm   Electron Image 1

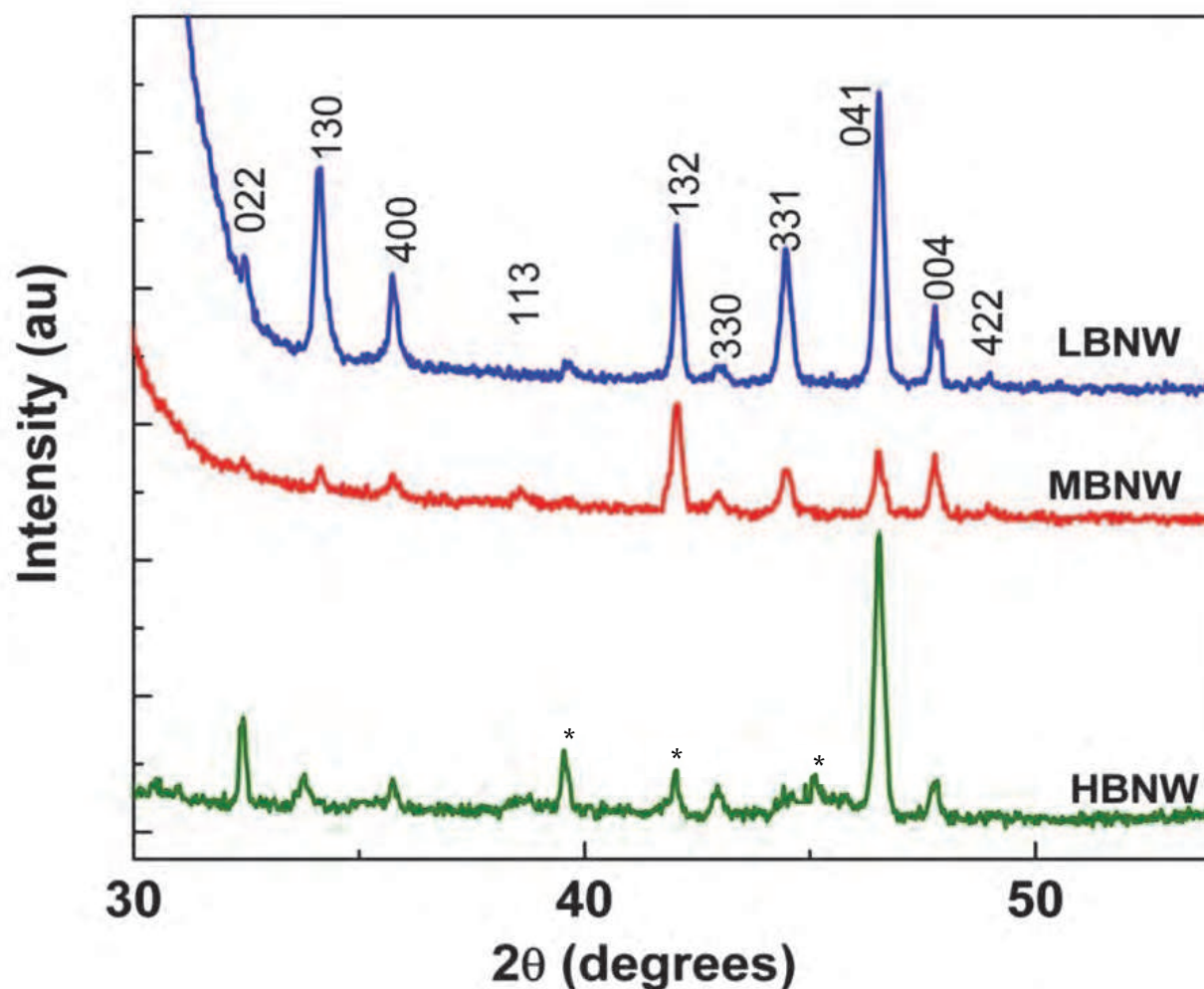Fig. 6. Scanning electron microscopy image of boron-incorporated Mn_5SiC nanowires.

Fig. 7. Xray diffraction patterns of boron-incorporated nanowires grown different silicon substrates (a) LBNW (b) MBNW and (c) HBNW. The peaks corresponding to Au_5Si_2 phase are marked.

remained uniform over the entire length of the nanowire. In order to understand whether the boron actually goes into the nanowire, we have carried out Secondary Ion Mass Spectroscopy studies (SIMS). A cleaning procedure was carried out to make sure that the surface of the nanowires is clean of any residues. In this process, the as-grown nanowires were etched for a short time in 5% HF solution. The nanowires from the as-grown substrates are removed using sonication and are transferred to an undoped silicon substrate for SIMS analysis. The undoped substrate avoids any boron signal from the substrate as in the case of the substrates that are used for the nanowire growth. SIMS sputter profiling analysis was performed using a 100 nA, 17 keV, $^{16}O^-$ primary beam with a square raster of 250 µm. Figure 8 displays the SIMS data for low and heavy boron-incorporated nanowires, which clearly indicate that the boron-intensity from HBNW's is strong, compared to the other. Thus, this confirms the presence of boron in the nanowires and the signal that is detected purely arises from the highly dispersed nanowire cluster. A quantitative estimate was difficult because of the unavailability of a boron standard for this particular measurement.
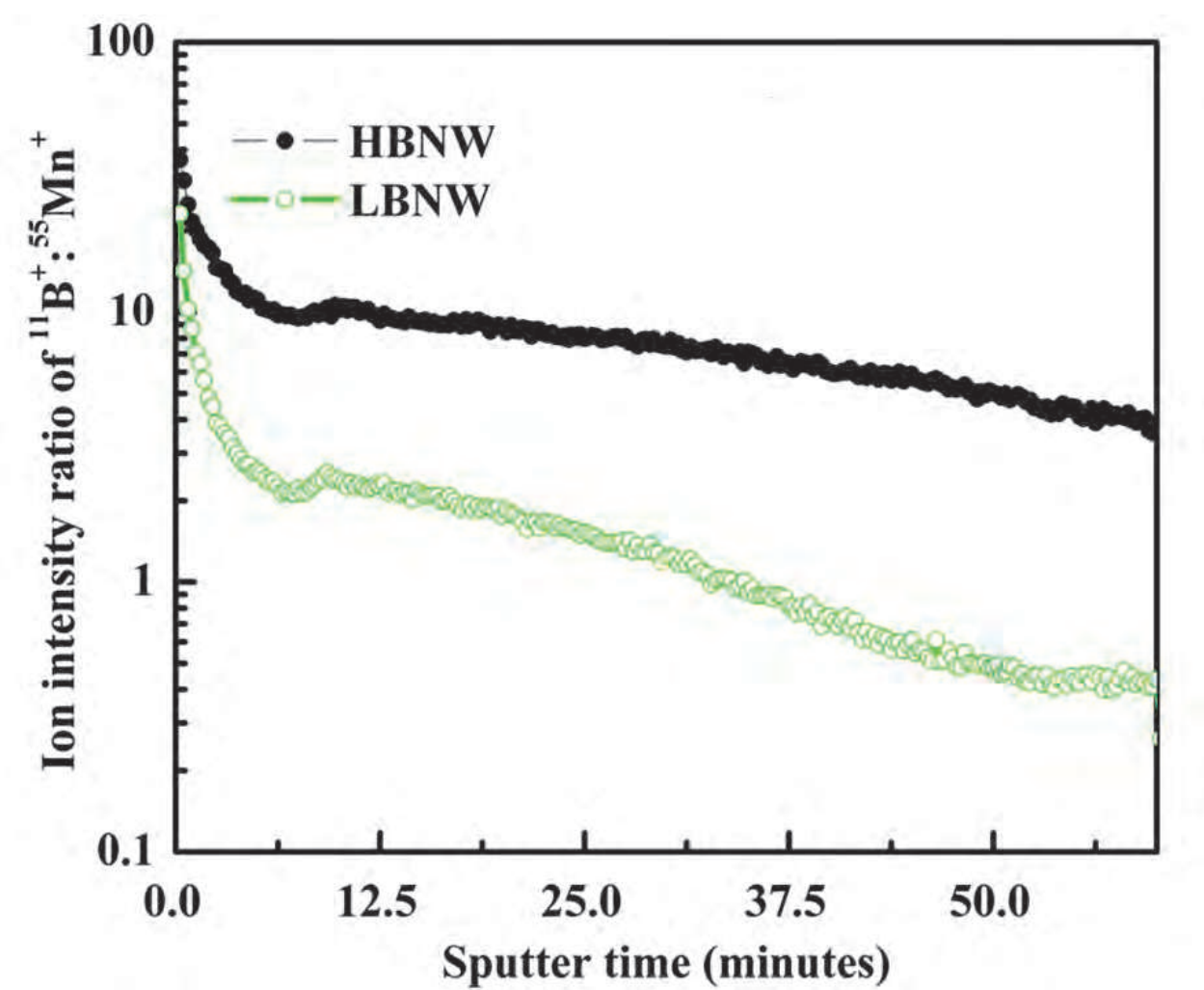
Fig. 8. SIMS data for LBNW and HBNW nanowires.

2.3.1 Magnetic properties

The magnetic hysteresis loops were measured using a superconducting quantum interference device (SQUID) magnetometer; the data for three different samples are displayed in Figure 9. The nanowires grown from low boron-doped silicon substrate exhibit higher saturation magnetization at room temperature. On the other hand, heavily boron-incorporated nanowires show very weak remanence; it is reduced by almost a factor of eight compared to the low-boron-incorporated nanowires. All of the three sets of nanowires exhibit magnetic hysteretic behavior at low temperature (15 K) with decreasing saturation magnetic moment as the boron incorporation increases. Thus, it is evident that the boron incorporation weakens the magnetic exchange interaction in Mn_5SiC nanostructures. We have measured the hysteresis loops up to 400 K, the low boron-doped sample exhibits clear hysteresis even at 400 K. Thus, the Curie temperature of these nanowires is higher than 400 K. Magnetic studies on thin films of $Mn_5Si_3C_x$ has shown that they exhibit finite magnetic moments even above room temperature (Sürgers et al., 2003). There is no theoretical studies exist to compare our experimental results, most of the simulation studies are on Mn doped silicon.
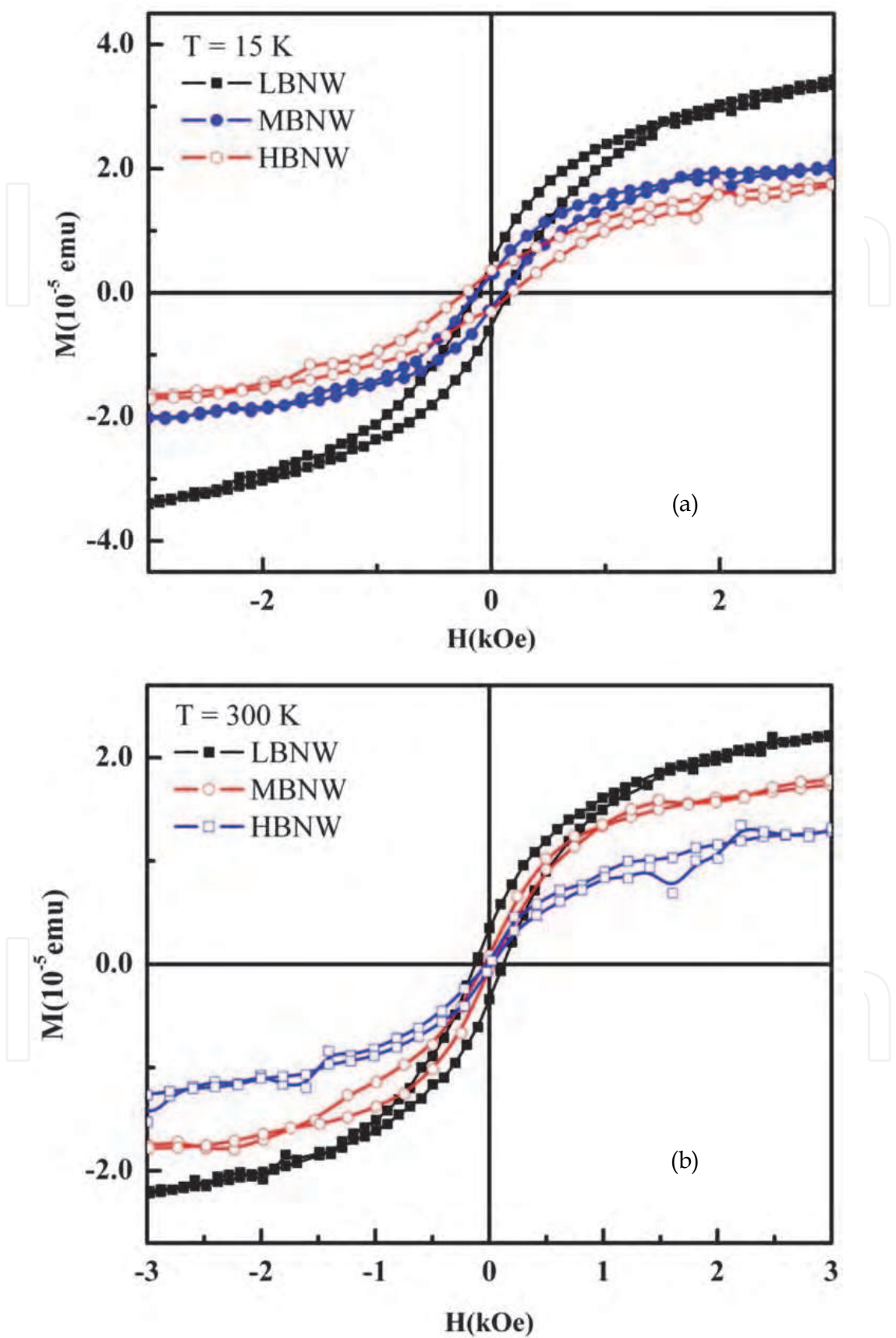
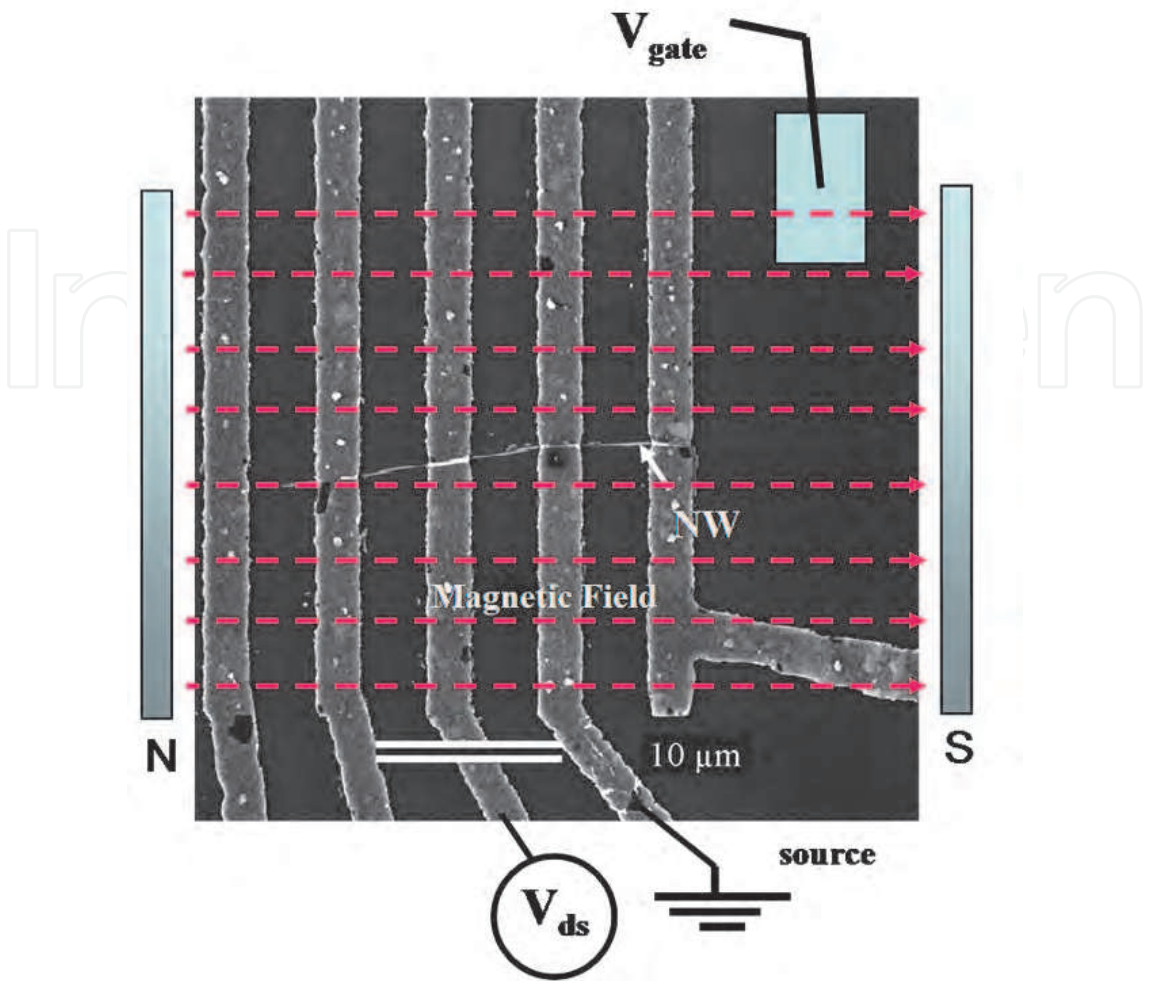Fig. 9. The magnetic hysteresis loops of the three sets of nanowires at (a) 15 and (b) 300 K

Fig. 10. SEM image of a typical nanowire device. The red lines indicate the direction of applied magnetic field. N and S denote the north and south poles of the magnet used for the measurement.
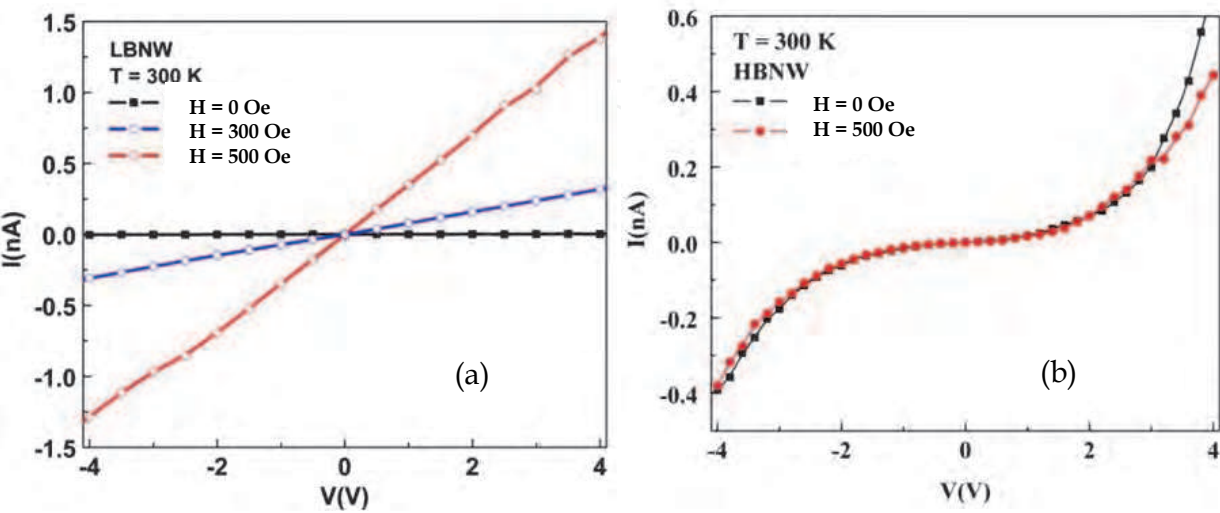

Fig. 11. Current-voltage characteristics of (a) LBNW and (b) HBNW nanowire devices with and without the presence of external magnetic fields.

2.3.2 Mn$_5$SiC nanowire devices

Nanowire devices are fabricated (Figure 10) with standard electron beam lithography for electrical and magneto-transport measurements. The electrodes on the nanowire channels are layers of Al(100 nm)/Au (5 nm) evaporated using an ultra-high vacuum thin film deposition system. The current-voltage (I-V) measurements were carried out using a semiconductor parametric analyzer show metallic (linear) and semiconducting (nonlinear) behaviors for the devices fabricated with LBNW and HBNW's as displayed in Figures 11(a) and (b). This is further confirmed by measuring the resistance of the nanowire devices as a function of temperature. In the presence of small external magnetic fields applied along the axial direction of the nanowires (H= 300 – 1000 Oe), there is a large change in the I-V characteristics in the case of a device fabricated with LBNW's. The change is almost two orders of magnitude, but there is a insignificant change in the case of devices with HBNW's, except for a small change at higher bias voltages. The electrical behavior, resistance of individual nanowire is measured as a function of temperature using a cryoprobe. The temperature dependence of resistance is plotted in Figure 12, it shows that the LBNW devices exhibit metallic behavior on the other hand the HBNW devices show strong semiconducting behavior. The LBNW devices display almost six orders of magnitude change in resistance. The magnetoresistance values (Figure 13) calculated from the I-V characteristics are much larger for the LBNW device and decreases for other devices as the saturation magnetization weakens. The magnetoresistance (MR) is calculated using the expression $[(R_{H=0\ Oe} – R_{H=500\ Oe})/R_{H=500\ Oe}]$. The MR value is very high, ~400 (40,000 %) for the low-boron-doped nanowire device and it is nearly negligible for the HBNW device.
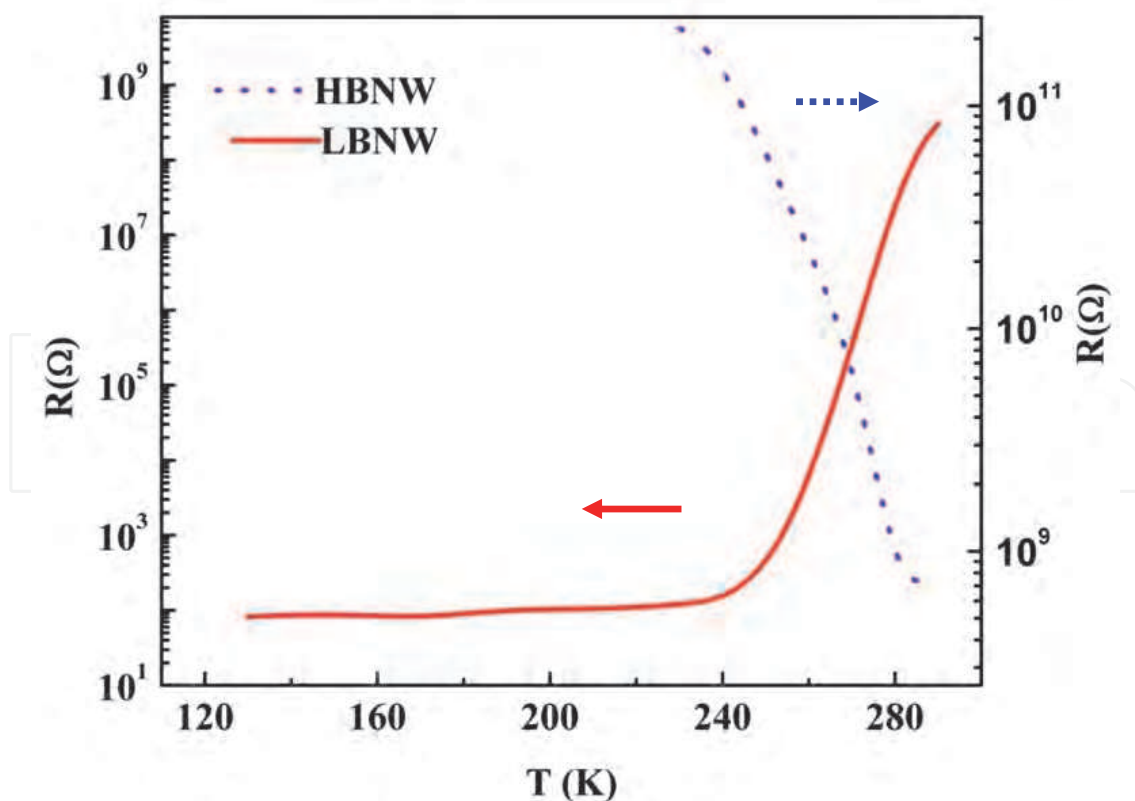

Fig. 12. Resistance vs temperature plots of the LBNW and HBNW nanowire devices exhibiting metallic and semiconducting behaviors.
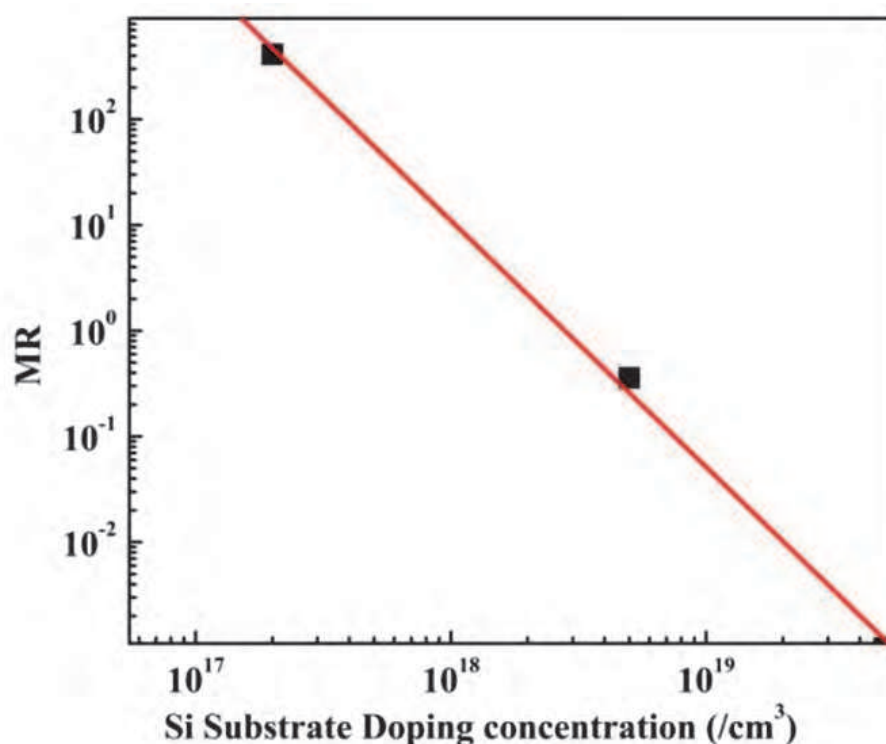
Fig. 13. Magnetoresistance of the nanowire devices decreases with the incorporation of boron. The x-axis gives the boron concentration of the silicon substrate used for the nanowire growth.

Comparing the magnetization, electrical and magneto-transport properties of the nanowires and their devices, nanowires that display strong magnetic behavior exhibit metallic behavior and huge magnetoresistance. Large incorporation of boron into the nanowires switches the electrical behavior to semiconducting, decreases the magnetic coupling and in turn considerably reduces the magnetoresistance.

2.4 Higher manganese silicide nanowires

In addition to manganese monosilides and silicide carbides, another interesting class is the higher manganese silicides (HMS). There is a series of crystallographically distinct phases called as Nowotny chimney ladder (NCL) phases. NCL phases correspond to chimneys of manganese atoms with ladders of Si atoms. The four commensurate NCL phases which are reported in the literature are Mn_4Si_7, $Mn_{11}Si_{19}$, $Mn_{15}Si_{26}$ and $Mn_{27}Si_{47}$. It is predicted that the electronic properties of these phases depend on the valence electron configuration and the metallic and semiconducting nature are predicted. Semiconducting higher manganese silicides are $MnSi_{2-x}$ and $MnSi_{1.75}$. There are no reports about the magnetic properties of the higher manganese silicides; it is shown that they are good thermoelectric materials. Higgins et al. (Higgins et al., 2008) have synthesized $Mn_{19}Si_{33}$ nanowires using $Mn(CO)_5SiCl_3$ precursor. These nanowires are grown using a CVD system and the mechanism of the nanowire growth is not well understood. In their CVD synthesis precursor used has a Mn/Si ratio of 1:1, but the nanowires grown have a Mn/Si ratio of 1:1.75. They have observed metallic behavior and no magnetoresistance effect for the $Mn_{19}Si_{33}$ nanowire device.

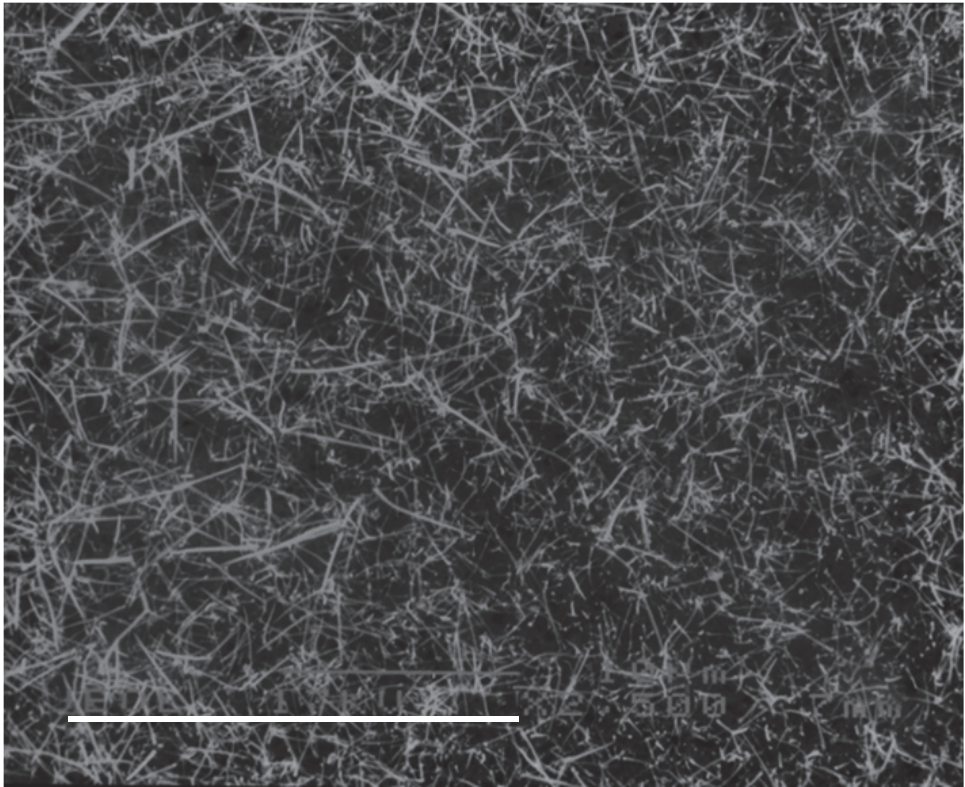Fig. 14. Scanning electron microscopy image of $Mn_{15}Si_{26}$ nanowires. Scale bar, 10 micrometers.
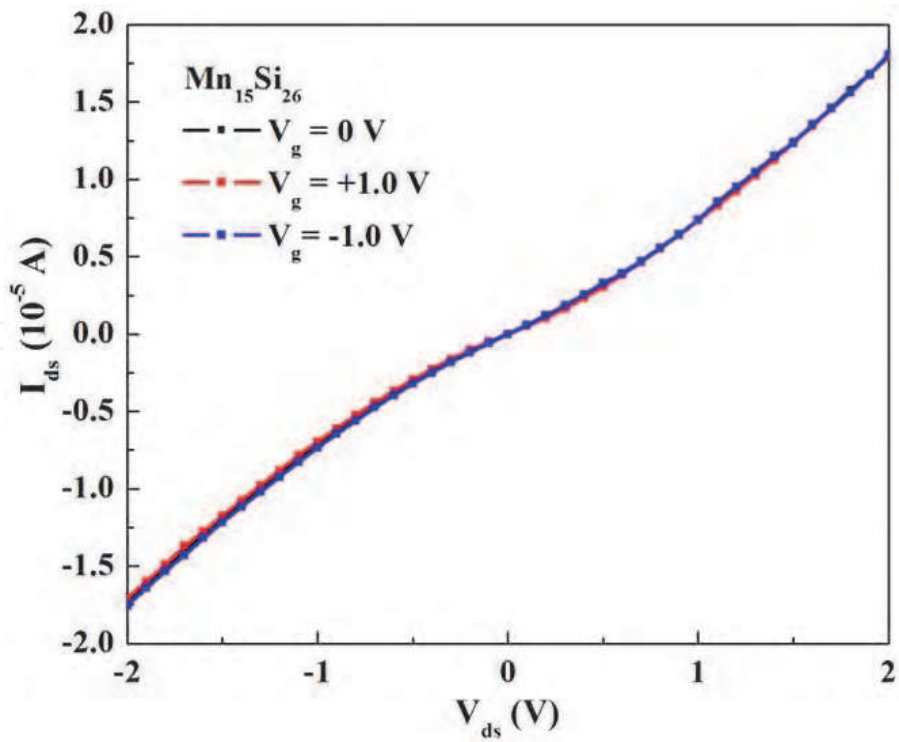

Fig. 15. Current- voltage characteristics of a typical $Mn_{15}Si_{26}$ nanowire device. It shows p-type semiconducting behavior.

We have grown $Mn_{15}Si_{26}$ nanowires using Mn-based beta diketone chelate precursor. The precursor is shown Fig 1(a). The growth method is similar to what is described earlier. In the CVD method we have grown the nanowires at 1050 °C for 2 hr. The wire size ranges from 80 – 200 nm and lengths up to hundreds of microns. Figure 14 shows the morphology of the wires. The x-ray diffraction analyses show that the nanowires exhibit the crystal structure of $Mn_{15}Si_{26}$ which is also supported by the selected area diffraction pattern from transmission electron microscopy. Nanoscale devices are fabricated using electron beam lithography and we have measured the electrical transport properties as displayed in Fig 15. It clearly shows that the nanowire is semiconducting with p-type behavior. The gate-effect is not significant probably due to the degenerate character of $Mn_{15}Si_{26}$ system.

3. Conclusions

Thus in conclusion, we have made use of manganese diketone chelates as precursors to grow different silicides. For the first time we have grown $Mn_{15}Si_{26}$ nanostructures and shown that nanowires exhibit p-type semiconducting behavior as reported in the literature for bulk $Mn_{15}Si_{26}$ system.

4. Acknowledgements

5. References

Aeppli, G. & DiTusa, J. F. (1999). Undoped and doped FeSi or how to make a heavy fermion metal with three of the most common elements. *Mater. Sci. Eng., B*, 63, 119–124

Aylett, B. J. & Colquhoun, H. M. (1977). Chemical vapour deposition of transition-metal silicides by pyrolysis of silyl transition-metal carbonyl compounds. *J. Chem. Soc., Dalton Trans.*, 2058–2061

Belitz, D.; Kirkpatrick, T. R. & Vojta, T. (1999). First Order Transitions and Multicritical Points in Weak Itinerant Ferromagnets. *Phys. Rev. Lett.* 82, 4707

Borisenko, V. E. (2000). *Semiconducting silicides*, Springer-Verlag, ISBN 3-540-66111-5

Brown, P. & Forsyth, J. (1995). Antiferromagnetism in Mn_5Si_3: the magnetic structure of the AF2 phase at 70 K .*J. Phys.: Condens. Matter.* 7, 7619

Cotton, F. A. & Holm, R. H. (1960). Magnetic Investigations of Spin-Free Cobaltous Complexes. III. On the Existence of Planar Complexes. *J. Am. Chem. Soc. 82*, 2979

Cullity, B. B. (1977). *Elements of X-Ray Diffraction.* Addison Wesley, ISBN: 0201610914, Massachusetts

Flieher, G.; Voellenkle, H. & Nowotny, H. (1967). Mangansilicide vom Typ $Mn_nSi_{2n-m.}$ *Monatsh. Chem. 98*, 2173–9

Gates, B.; Mayers, B.; Cattle, B.. & Xia, Y. (2002). Synthesis and Characterization of Uniform Nanowires of Trigonal Selenium. *Adv. Funct. Mater.* 12, 219–27

Higgins, J. M.; Schmitt, A. L.; Guzei, I. A. and Jin, S. (2008). Higher Manganese Silicide Nanowires of Nowotny Chimney Ladder Phase. *J. Am. Chem. Soc. 130,* 16086-16094

Ishikawa, Y.; Tajima, K.; Bloch, D. & Roth, M. (1976). Helical spin structure in manganese silicide MnSi. *Solid State Commun.* 19, 525

Kang, S.; Brewer, G. A.; Battogtokh, J.; DiPietro, R.; Heiman, D.; Buechele, A. C.; McKeown, D. A.; Pegg, I. L.; Philip, J. (2009). Growth and Characterization of Mn_5SiC nanowires. *Nanotech. Nanosci. Lett.* 1(2), 77

Kang, S.; Brewer, G. A.; Jugdersuren, B.; DiPietro, R.; Heiman, D.; Buechele, A. C.; McKeown, D. A.; Pegg, I. L. & Philip, J. (2010). Magnetotransport properties of Mn-Si-C based nanostructures, *J. Appl. Phys.* 107(10), 104503

Kruyt, H. R. & Arkel, A. E. V.; (1928). Die Ausflockungsgeschwindigkeit des Selensols. *Colloid & Polymer Science,* 32, 29-36

Kusaka, S.; Yamamoto, K.; Komatsubara, T. & Ishikawa, Y. (1976). Ultrasonic study of magnetic phase diagram of MnSi. *Solid State Commun.* 20, 925

Lander, G. H.; Brown, P. J. & Forsyth, J. B. (1967). The antiferromagnetic structure of Mn_5Si_3. *Proc. Phys. Soc.London,* 91, 332

Maex, K. & van Rossum, M. (Eds.), (1995). *Properties of Metal Silicides,* INSPEC, ISBN-10: 0852968590, London

Mayers, B. & Xia, Y. (2002). One-dimensional nanostructures of trigonal tellurium with various morphologies can be synthesized using a solution-phase approach. *J. Mater. Chem.* 12, 1875–81

Messer, B.; Song, J.H.; Huang, M.; Wu, Y.; Kim, F. & Yang, P. (2000). Surfactant-Induced Mesoscopic Assemblies of Inorganic Molecular Chains. *Adv. Mater.* 12, 1526–1528

Miglio, L. & d'Heurle, F. (2001). *Silicides: Fundamentals and Applications*, World Scientific Publishing Company, ISBN 981-02- 4452-5

Murarka, S. P. (1983). *Silicides for VLSI Applications*, Academic Press, Inc. ISBN-10: 0125112203, Florida

Novak, I.; Huang, W.;Luo, L.; Huang, H. H.; Ang , H. G. & Zybill, C. E. (1997). UPS Study of Compounds with Metal−Silicon Bonds: $M(CO)_nSiCl_3$ (M = Co, Mn;n = 4, 5) and $Fe(CO)_4(SiCl_3)_2$. *Organometallics,* 16, 1567–1572

Pfleiderer, C.; Böni, P.; Keller, T.; Rößler, U. K. & Rosch, A. (2007). Non-Fermi Liquid Metal without Quantum Criticality.*Science,* 316, 1871

Riseborough, P. S. (2000). Heavy fermion semiconductors. *Adv. Phys.* 49, 257–320

Schmitt, A. L.; Higgins, J. M.; Szczech, j. R. & Song J. (2010). Synthesis and applications of metal silicide nanowires. *J. Mater. Chem*. 20, 223–235

Schwomma, O.; Preisinger, A.; Nowotny, H. & Wittmann, A. (1964). Die Kristallstruktur von $Mn_{11}Si_{19}$ und deren Zusammenhang mit Disilicid-Typen. *Monatsh. Chem.* 95, 1527–37

Sénateur, J. P.; Bouchaud, J. –P. & Fruchart, R. (1967). Study of non- stoichiometric effects in compounds Mn5Si3 and Mn3GaC1-x . *Bull. Soc. Fr. Mineral. Cristallogr.* 90, 537

Silva, M. R.; Brown, P. J. & Forsyth, J. B. (2002). Magnetic moments and magnetic site susceptibilities in Mn_5Si_3. *J. Phys.: Condens.Matter* 14, 8707

Song, J.; Messer, B.;, Wu, Y.; Kind, H. & Yang, P. (2001). MMo3Se3 (M = Li$^+$, Na$^+$, Rb$^+$, Cs$^+$, NMe$_4$$^+$) Nanowire Formation via Cation Exchange in Organic Solution. *J. Am. Chem. Soc.* 123, 9714–9715

Stejny, J. J.; Trinder, R.W. & Dlugosz, J. (1981). Preparation and structure of poly (sulphur nitride) whiskers. *J Mater Sci.* 16, 3161–70.

Stejny, J. J.; Dlugosz, R.W. & Keller, A. (1979). Electron microscope diffraction characterization of the fibrous structure of poly (sulphur nitride) crystals. *J Mater Sci.* 14, 1291–300

Stishov, S. M.; Petrova, A. E.; Khasanov, S.; Panova, G. K.; Shikov, A. A.; Lashley, J. C.; Wu, D. & Lograsso, T. A. (2007). Magnetic phase transition in the itinerant helimagnet MnSi: Thermodynamic and transport properties. *Phys. Rev. B,* 76, 052405

Sürgers, C.; Gajdzik, M.; Fischer, G.; Löhneysen, H. v.; Welter, E. & Attenkofer, K. (2003). Preparation and structural characterization of ferromagnetic Mn$_5$Si$_3$C$_x$ films. *Phys. Rev. B* 68, 174423

Vining, C. B. (1995). *CRC handbook of Thermoelectrics*, Ed., D. M. Rowe, CRC Press, 277, ISBN: 0849301467

Wagner, R. S. & Ellis, W. C. (1964). Vapor-Liquid-Solid Mechanism of Single Crystal Growth. *Appl. Phys. Lett.* 4, 89–91

Wagner, R. S. (1970). Growth of whiskers by vapor-phase reactions, In: *Whisker technology* (ed. A. P. Levitt), ch. 2, pp. 15–119, Wiley-Interscience, ISBN 10: 0471531502, New York

Walker, W. R; Li, N. C. (1965). 4-methyl-pyridine adducts of copper (II) β-diketone chelates. *J. Inorg. Nucl. Chem.* 27(10), 2255-2261

Xia, Y.; Yang, P.; Sun, Y.; Wu, Y.; Mayers , B.; Gates, B.; Yin, Y.; Kim, F. & Yan, H. One-Dimensional Nanostructures: Synthesis, Characterization, and Applications. *Adv. Mater.* 15, (2003), 353–389

Nanowires - Fundamental Research

Edited by Dr. Abbass Hashim

Understanding and building up the foundation of nanowire concept is a high requirement and a bridge to new technologies. Any attempt in such direction is considered as one step forward in the challenge of advanced nanotechnology. In the last few years, InTech scientific publisher has been taking the initiative of helping worldwide scientists to share and improve the methods and the nanowire technology. This book is one of InTech's attempts to contribute to the promotion of this technology.

How to reference

In order to correctly reference this scholarly work, feel free to copy and paste the following:

John Philip (2011). Silicide Nanowires from Coordination Compound Precursors, Nanowires - Fundamental Research, Dr. Abbass Hashim (Ed.), ISBN: 978-953-307-327-9, InTech, Available from: http://www.intechopen.com/books/nanowires-fundamental-research/silicide-nanowires-from-coordination-compound-precursors

INTECH
open science | open minds